Available online at www.sciencedirect.com

ScienceDirect

Proceedings of the Combustion Institute 000 (2020) 1–8

Proceedings of the Combustion Institute

www.elsevier.com/locate/proci

A localized thickened flame model for simulations of flame propagation and autoignition under elevated pressure conditions

Hiroshi Terashima [a,*], Yutaka Hanada [b], Soshi Kawai [b]

[a] *Division of Mechanical and Aerospace Engineering, Hokkaido University, N13 W8, Kita-ku, Sapporo, Hokkaido 060–8628, Japan*

[b] *Department of Aerospace Engineering, Tohoku University, 6-6-01, Aramaki-Aza-Aoba, Aoba-ku, Sendai, Miyagi 980–8579, Japan*

Received 8 November 2019; accepted 7 June 2020
Available online xxx

Abstract

The present study proposes a localized thickened flame (LTF) model for the accurate prediction of flame propagation and autoignition timing. The unresolved-scale terms appeared in spatially-filtered governing equations due to thin flame structures are constructed under a physical constraint in which laminar flame speed is maintained. A high-order derivative is introduced to dynamically localize the effects of the LTF in the regions of unresolved propagating flame. The model is also designed such that the thickened flame is resolved by the same number of grid points for any grid size used. Therefore, a user-specified constant in the model does not need to be adjusted depending on the employed grid size. Laminar flame propagation problems are used to validate the performance of the proposed LTF model and determine the appropriate value of the user-specified constant. The results using a one-dimensional constant-volume reactor demonstrate that the LTF successfully captures the accurate flame propagation behaviors under elevated pressure conditions, while not affecting the end-gas autoignition timing, even on relatively coarse grid resolutions. The high-order derivative in the LTF serves as a dynamic parameter for detecting the thinning flame under elevated pressure conditions.

Keywords: Thickened flame model; Flame propagation; Autoignition; Knocking combustion

1. Introduction

Demand for predicting accurate and detailed combustion flow fields has grown with the need to improve thermal efficiency and reduce greenhouse gas emissions. High-fidelity combustion flow simulation is certainly a promising tool for predicting

* Corresponding author.
E-mail address: htera@eng.hokudai.ac.jp (H. Terashima).

https://doi.org/10.1016/j.proci.2020.06.063

and controlling combustion flow fields. In such simulations, chemical kinetics play a significant role in combustion phenomena. Recently, several attempts have been made to introduce large detailed reaction mechanisms in combustion flow simulations to improve the prediction capability of chemical kinetics. For example, some time integration methods [1–3] have been developed to efficiently solve stiff chemical reaction equations having detailed reaction mechanisms.

Although the use of detailed reaction mechanisms can provide detailed and useful information about combustion flow fields (i.e., chemical reaction behavior), a large number of grid points is required to resolve the structure of a propagating flame. This is because flame thickness is an order of 10^{-2} cm, even under atmospheric conditions; the thickness gets much thinner under increasing surrounding pressures. Thus, direct numerical simulations (DNS), where a flame structure is fully resolved using computational grids, are extremely difficult for large-scale three dimensional problems. On the other hand, large-eddy simulation (LES) is a promising approach in terms of prediction accuracy and computationally required loads. However, for combustion LESs, the spatial filtering for the production rate of chemical species is essentially difficult because of the exponential form of the Arrhenius equation. Thus, a probability density function method [4], a conditional momentum closure model [5], a linear-eddy model [6], and artificially thickened flame (TF) models [7,8] have been proposed in the context of combustion LESs with detailed chemical kinetics. However, unfortunately, there is still an issue that no standard model has been established because of the difficulty constructing the spatial filter of the production rate based on the Arrhenius equation.

Among those models, TF models [7,8] offer the direct use of detailed reaction mechanisms and it can be easily introduced to the Navier–Stokes equations with no major modifications. The production rate of chemical species is directly calculated using a detailed reaction mechanism. In the TF model, a thickening factor is introduced to the diffusion terms of species so that a flame thickness is artificially diffused and properly resolved by a relatively coarse computational grid. However, in the model, the production rate is reduced by the thickening factor to approximately maintain laminar flame speeds. The progress of chemical reactions is accordingly affected, even in a region apart from the flame front. Therefore, several studies [9–12] have been conducted to alleviate the unfavorable effects of the thickening factor on chemical reaction behaviors. For example, Proch [11] modified the thickening factor by using a flame sensor to localize the effect of the thickening factor in a region near the flame front. Schulz et al. [12] introduced an autoignition index using reaction rates as an indicator to distinguish an autoignition region from a flame front. However, most studies seemingly focused only on the detection of a flame front; little attention was paid to the performance of autoignition phenomena, including the prediction of autoignition timing.

In some combustion problems in a confined space, a flame propagates under elevated pressure conditions, indicating that the flame thickness dynamically changes. Thus, the thickening factor should be adjusted for the changes of flame thickness. However, the thickening factor in most TF models is determined in *a priori* manner, and therefore significant uncertainty still exists in the determination of the thickening factor under elevated pressure conditions. Hence, TF models have been little applied to the simulations of flame propagation under elevated pressure conditions. This kind of flame propagation is important to internal combustion engines and the prediction of their autoignition timing.

The present study proposes a new flame model applicable to the prediction of not only flame propagation under elevated pressure conditions, but also autoignition timing. The model derivation is based on the spatially-filtered equations, where the terms emerged due to unresolved scales are consistently constructed by imposing a physically constrained condition, which is a different concept from previous TF models [7–12]. Note that this study is the first attempt to derive the terms associated with thin flame structures in the context of a TF model. Thus, turbulence effects are not considered.

2. Numerical methods

2.1. Governing equations

The governing equations are the compressible Navier–Stokes equations with the mass conservation equations of chemical species. A thermally perfect gas is assumed. As with conventional LES equations [13], the spatially-filtered form of the governing equations is written as follows:

$$\frac{\partial \bar{\rho}}{\partial t} + \nabla \cdot (\bar{\rho}\tilde{\boldsymbol{u}}) = 0, \tag{1}$$

$$\frac{\partial \bar{\rho}\tilde{\boldsymbol{u}}}{\partial t} + \nabla \cdot (\bar{\rho}\tilde{\boldsymbol{u}} \otimes \tilde{\boldsymbol{u}} + \bar{p}\boldsymbol{\delta} - \bar{\boldsymbol{\tau}}) = 0, \tag{2}$$

$$\frac{\partial \bar{E}}{\partial t} + \nabla \cdot \left[(\bar{E} + \bar{p})\tilde{\boldsymbol{u}} - \bar{\boldsymbol{\tau}} \cdot \tilde{\boldsymbol{u}} + \bar{\boldsymbol{q}}\right] = 0, \tag{3}$$

$$\frac{\partial (\bar{\rho}\tilde{Y}_s)}{\partial t} + \nabla \cdot \left[\bar{\rho}\tilde{Y}_s\tilde{\boldsymbol{u}} - \bar{\boldsymbol{d}}_s\right] = \bar{\dot{\omega}}_s, \tag{4}$$

$$\bar{p} = \bar{\rho} R \sum_{s=1}^{N} (\tilde{Y}_s / M_s)\tilde{T}, \tag{5}$$

Please cite this article as: H. Terashima, Y. Hanada and S. Kawai, A localized thickened flame model for simulations of flame propagation and autoignition under elevated pressure conditions, Proceedings of the Combustion Institute, https://doi.org/10.1016/j.proci.2020.06.063

where ρ is the density, $\boldsymbol{u}$ is the velocity vector, E is the total energy, p is the pressure, T is the temperature, and R is the universal gas constant. $\boldsymbol{\tau}$ is the viscous stress tensor, $\boldsymbol{q}$ is the heat flux vector, and $\boldsymbol{\delta}$ is the unit tensor. Y_s, $\boldsymbol{d}_s$, M_s, and $\dot{\omega}_s$ are the mass fraction, the diffusion vector, the molar mass and the production rate of species s, respectively. N is the total number of species. The bar $\bar{(\cdot)}$ indicates Reynolds-filtered quantities, and the tilde $\tilde{(\cdot)}$ indicates Favre-filtered quantities [13]. Note that the spatially-filtered production rate of species is not directly obtained by the filtered quantities in general, $\bar{\dot{\omega}}_s \neq \dot{\omega}_s(\bar{\rho}, \tilde{T}, \tilde{Y}_s)$.

The spatially-filtered viscous stress tensor is represented as follows:

$$\bar{\boldsymbol{\tau}} = \bar{\mu}\left(2\bar{\boldsymbol{S}} - 2/3(\nabla \cdot \tilde{\boldsymbol{u}})\boldsymbol{\delta}\right), \tag{6}$$

where μ is the viscosity of mixtures and $\boldsymbol{S}$ is the symmetric strain tensor. Here, $\bar{\mu} = \breve{\mu} + \mu_{\mathrm{urs}}$, where the breve $\breve{(\cdot)}$ indicates that the variable is calculated using Reynolds- and Favre-filtered quantities and the subscript $(\cdot)_{\mathrm{urs}}$ denotes that the term includes the effects of unresolved scales. The spatially-filtered heat flux vector is represented as follows:

$$\bar{\boldsymbol{q}} = -\bar{\kappa}\nabla\tilde{T} - \sum_{s=1}^{N} \tilde{h}_s \bar{\boldsymbol{d}}_s, \tag{7}$$

where $\bar{\kappa} = \breve{\kappa} + \kappa_{\mathrm{urs}}$ and κ is the thermal conductivity of mixtures. h_s is the enthalpy of each species. The diffusion vector $\boldsymbol{d}_s$ is modeled as

$$\bar{\boldsymbol{d}}_s = \bar{\rho}\bar{D}_s\nabla\tilde{Y}_s, \tag{8}$$

where $\bar{D}_s = \breve{D}_s + D_{s,\mathrm{urs}}$ and D_s is the diffusion coefficient of each species.

The spatially-filtered production rate, which is key to the LES of reactive flows, is assumed to be modeled as follows:

$$\bar{\dot{\omega}}_s = \breve{\dot{\omega}}_s + (\bar{\dot{\omega}}_s - \breve{\dot{\omega}}_s) = \breve{\dot{\omega}}_s + \dot{\omega}_{s,\mathrm{urs}}, \tag{9}$$

where we define that, in contrast to $\bar{\dot{\omega}}_s$, the first term in the right-hand side is the production rate of species calculated using the filtered quantities, $\breve{\dot{\omega}}_s = \dot{\omega}_s(\bar{\rho}, \breve{T}, \tilde{Y}_s)$. The second term represents the effects of unresolved scales. Details on the numerical methods and models for solving the governing equations can be found in [14], and also provided in the supplementary material.

2.2. Flame modeling

2.2.1. Constructing unresolved flame components

The terms associated with unresolved scales in Eqs. (6)–(9) are constructed under a physically constrained condition. Following the idea of the TF model [7,8], this study uses laminar flame speed as a constraint. According to the theoretical analysis for a steady premixed flat flame [15], the laminar flame speed may be proportional to the square root of $\dot{\omega}_s D_s$, $\dot{\omega}_s \kappa$, and $\dot{\omega}_s \mu$.

We consider a local (laminar) flame speed $s_L(x)$ in 1-D flame. For a part of an LES flame, an average, $\langle f \rangle_{\mathrm{LES}} \equiv \frac{1}{\Delta_{\mathrm{avg}}} \int_{\Delta_{\mathrm{avg}}} f \mathrm{d}x$, is introduced, while $\langle f \rangle_{\mathrm{DNS}}$ is defined as the average for the corresponding part of a DNS flame. Here we consider Δ_{avg} is the grid size employed in LES. To maintain correct s_L in LES, the following relationship should be satisfied between the corresponding parts of the DNS and LES flames,

$$\langle \dot{\omega}_s \rangle_{\mathrm{DNS}} \langle D_s \rangle_{\mathrm{DNS}} = \langle \breve{\dot{\omega}}_s + \dot{\omega}_{s,\mathrm{urs}} \rangle_{\mathrm{LES}} \langle \breve{D}_s + D_{s,\mathrm{urs}} \rangle_{\mathrm{LES}}, \tag{10}$$

where the left-hand side represents $\propto s_L^2$ obtained by DNS, in which the flame structures are fully resolved, and the right-hand side represents a corresponding s_L^2 computed on a coarse mesh with the LES Eqs. (1)–(4).

According to the TF model [7,8], the DNS term in Eq. (10) can be also obtained by using $\langle \breve{\dot{\omega}}_s \rangle_{\mathrm{LES}}$ and $\langle \breve{D}_s \rangle_{\mathrm{LES}}$ through a flame thickening operation, that is, $\langle \dot{\omega}_s \rangle_{\mathrm{DNS}} \langle D_s \rangle_{\mathrm{DNS}} = \frac{\langle \breve{\dot{\omega}}_s \rangle_{\mathrm{LES}}}{F} F \langle \breve{D}_s \rangle_{\mathrm{LES}} = \langle \breve{\dot{\omega}}_s \rangle_{\mathrm{LES}} \langle \breve{D}_s \rangle_{\mathrm{LES}}$ holds for maintaining correct s_L in LES, where F is usually denoted as a thickening factor. Therefore, if the unresolved-scale terms have a similar role to the flame thickening, Eq. (10) may turn to

$$\langle \breve{\dot{\omega}}_s \rangle_{\mathrm{LES}} \langle \breve{D}_s \rangle_{\mathrm{LES}} = \left(\langle \breve{\dot{\omega}}_s \rangle_{\mathrm{LES}} + \langle \dot{\omega}_{s,\mathrm{urs}} \rangle_{\mathrm{LES}} \right) \left(\langle \breve{D}_s \rangle_{\mathrm{LES}} + \langle D_{s,\mathrm{urs}} \rangle_{\mathrm{LES}} \right). \tag{11}$$

Similarly, for the thermal conductivity (hereafter the subscript LES is dropped off for brevity),

$$\langle \breve{\dot{\omega}}_s \rangle \langle \breve{\kappa} \rangle = \left(\langle \breve{\dot{\omega}}_s \rangle + \langle \dot{\omega}_{s,\mathrm{urs}} \rangle \right) \left(\langle \breve{\kappa} \rangle + \langle \kappa_{\mathrm{urs}} \rangle \right), \tag{12}$$

and the same holds for the viscosity.

To derive the unresolved-scale components, we first model $\langle D_{s,\mathrm{urs}} \rangle$ as

$$\langle D_{s,\mathrm{urs}} \rangle = \chi \langle \breve{D}_s \rangle, \tag{13}$$

assuming a similarity between $\breve{D}_s$ and $D_{s,\mathrm{urs}}$ under the gradient-diffusion hypothesis. An arbitrary function χ has a positive value and is assumed to be constant in an average interval Δ_{avg} for simplicity (while χ varies in space and time). Accordingly, the flame is thickened as the diffusion increases with $\langle \bar{D}_s \rangle = (1 + \chi)\langle \breve{D}_s \rangle$ in Eq. (8). Subsequently, substituting Eq. (13) into Eq. (11) provides a form of $\dot{\omega}_{s,\mathrm{urs}}$ as follows:

$$\langle \dot{\omega}_{s,\mathrm{urs}} \rangle = -(\chi/(\chi + 1))\langle \breve{\dot{\omega}}_s \rangle. \tag{14}$$

Then, the unresolved-scale components of the thermal conductivity and viscosity are obtained from Eq. (12) as

$$\langle \kappa_{\mathrm{urs}} \rangle = \chi \langle \breve{\kappa} \rangle \quad \text{and} \quad \langle \mu_{\mathrm{urs}} \rangle = \chi \langle \breve{\mu} \rangle, \tag{15}$$

respectively. Consequently, Eqs. (13)–(15) indicate that all the unresolved-scale components can be constructed with one single arbitrary function χ, and the proposed unresolved components maintain

Please cite this article as: H. Terashima, Y. Hanada and S. Kawai, A localized thickened flame model for simulations of flame propagation and autoignition under elevated pressure conditions, Proceedings of the Combustion Institute, https://doi.org/10.1016/j.proci.2020.06.063

correct s_L, while thickening the flame region by the factor of $(1+\chi)$.

Finally, we obtain approximate forms of Eqs. (13)–(15) as follows:

$$D_{s,\mathrm{urs}} = \chi \breve{D}_s, \quad \dot{\omega}_{s,\mathrm{urs}} = -(\chi/(\chi+1))\breve{\dot{\omega}}_s,$$
$$\kappa_{\mathrm{urs}} = \chi\breve{\kappa}, \quad \mu_{\mathrm{urs}} = \chi\breve{\mu}. \tag{16}$$

The derivation of Eq. (16) from Eqs. (13)–(15) is given in the supplementary material.

When χ is constant in space and time, the governing Eqs. (1)–(4) turns to the same form as the original TF model [7,8] by holding $\chi = F - 1$. Thus, the spatially-filtered governing Eqs. (1)–(4) with the unresolved-scale components (16) can be considered as the general form of the TF model. The current process of constructing the unresolved-scale components based on the filtered equations is different from that of the original TF model, where the non-filtered governing equations were directly modified using a thickening factor.

2.2.2. Determining an arbitrary function

The arbitrary function, χ, is the only parameter in the unresolved-scale components. Ideally, χ should be active in the regions where the flame is not well resolved and automatically deactivated where the flame is well resolved.

The present study introduces a localization property to χ. For the localization, the concept of localized artificial diffusivity methods [16,17] is applied. This has been used for compressible turbulent flow simulations to numerically capture shock waves (here we construct χ to capture flames). In this study, χ is modeled using a high-order derivative of temperature for flame identification, which is expressed as follows:

$$\chi = C_\chi \left(\frac{\Delta s_F}{\delta_L}\right)^n \sum_{i=1}^{3} \overline{\left|\frac{\partial^4}{\partial x_i^4}\left(\frac{T}{T_{\mathrm{ad}}}\right)\right|} \Delta x_i^4, \tag{17}$$

where C_χ is a dimensionless user-specified constant, and Δs_F is the grid size used for resolving a flame. δ_L and T_{ad} are a laminar flame thickness and an adiabatic flame temperature for a given condition, respectively. x_i refers to the Cartesian coordinates x, y, and z when i is 1, 2 and 3, respectively. Δx_i is the grid spacing in each direction. The overbar in Eq. (17) denotes an approximate truncated Gaussian filter [16]. When a flame is unresolved, the value of χ becomes large. Thus, the flame is preferably diffused through Eq. (13). On the other hand, when a flame is properly resolved by the grid used, χ is automatically deactivated ($\chi \to 0$), and thus the unresolved-scale components disappear. Accordingly, the original DNS equations are recovered.

In Eq. (17), the term, $(\Delta s_F/\delta_L)^n$, is introduced to attain a grid-independent property for the user-specified constant, C_χ. Here, we determine an exponent n under the condition that the thickened flame is resolved using the same number of grid points for any grid sizes.

Let δ_F denote a physical flame thickness, whereas $\delta_F^{'}$ denotes a numerically-diffused flame thickness resolved with a grid size of Δs_F. Also, $\delta_{mF}^{'}$ is defined as a numerically-diffused flame thickness resolved with a larger grid size of $m\Delta s_F$, where $m > 1$. In simulations, as a flame is thickened with the factor, $(1+\chi)$, the numerically-diffused flame thicknesses can be expressed as follows:

$$\delta_F^{'} = (1+\chi)\delta_F = \left(1 + C_\chi \left(\frac{\Delta s_F}{\delta_L}\right)^n \sum_{i=1}^{3} \overline{\left|\frac{\partial^4}{\partial x_i^4}\left(\frac{T}{T_{\mathrm{ad}}}\right)\right|} \Delta x_i^4\right)\delta_F, \tag{18}$$

$$\delta_{mF}^{'} = (1+\chi_m)\delta_F = \left(1 + C_\chi \left(\frac{m\Delta s_F}{\delta_L}\right)^n \sum_{i=1}^{3} \overline{\left|\frac{\partial^4}{\partial x_i^4}\left(\frac{T}{T_{\mathrm{ad}}}\right)\right|} \Delta x_i^4\right)\delta_F, \tag{19}$$

where χ_m is the function χ used for the larger grid size. Then, comparing the number of grid points N_g in a flame region for the grid size of Δs_F and N_{mg} for the larger grid size of $m\Delta s_F$ gives

$$\frac{N_{mg}}{N_g} = \frac{\delta_{mF}^{'}/(m\Delta s_F)}{\delta_F^{'}/\Delta s_F} \approx \frac{(1+m^n\chi)\delta_F/(m\Delta s_F)}{(1+\chi)\delta_F/\Delta s_F}, \tag{20}$$

where since we design the LTF model such that the flame is represented using the same number of grid points, we may assume that the high-order derivative of temperature is approximately identical between the two flames.

The concept of the present model is to numerically diffuse a flame, and thus m is sufficiently large and χ accordingly becomes large. Therefore, Eq. (20) reduces to

$$N_{mg}/N_g \approx \left(m^{n-1}\chi\right)/\chi = m^{n-1}. \tag{21}$$

Consequently, the exponent, $n = 1$, is approximately obtained to satisfy the condition, $N_{mg} = N_g$, in which the flame is resolved with the same number of grid points, even with the different grid sizes. Finally, the arbitrary function, χ, is given as

$$\chi = C_\chi \left(\frac{\Delta s_F}{\delta_L}\right) \sum_{i=1}^{3} \overline{\left|\frac{\partial^4}{\partial x_i^4}\left(\frac{T}{T_{\mathrm{ad}}}\right)\right|} \Delta x_i^4, \tag{22}$$

where, as demonstrated in the results below, T_{ad} and δ_L are preliminary specified using initial conditions. Thinning flames during simulations can be detected by the high-order derivative of temperature. Thus, C_χ is the only parameter in the model, which should be a grid-independent value. C_χ is

Please cite this article as: H. Terashima, Y. Hanada and S. Kawai, A localized thickened flame model for simulations of flame propagation and autoignition under elevated pressure conditions, Proceedings of the Combustion Institute, https://doi.org/10.1016/j.proci.2020.06.063

thus determined in simulations of laminar flame propagation in a following section.

In contrast to other TF models [7–12], the present flame model may be referred to as a localized TF (LTF) model from the localization property.

3. Results and discussions

One-dimensional (1-D) laminar flame propagation problems are used to determine the dimensionless user-specified constant, C_χ, and to validate the fundamental performance of the LTF. Then, we apply the LTF to a 1-D autoignition and flame propagation problem in an open space, and finally a 1-D constant-volume reactor model [14,18] is used to demonstrate the capability of the LTF on the prediction of both flame propagation and autoignition under elevated pressure conditions. The supplementary material provides two-dimensional results to demonstrate the multi-dimensional capability and superiority of the LTF model.

3.1. Laminar flame propagation in an open space

A stoichiometric CH_4/air premixed mixture is considered. The flame propagates freely in an open space on a computational domain of $-L/2 \le x \le L/2$, where a large length of $L = 80$ m is used to minimize the boundary effects. The Dirichlet condition is imposed on the left and right boundaries. A uniform grid size is used for $|x| \le 12$ cm, and the grid spacing is coarsened toward the boundary. The unburned premixed gas and the corresponding gas at adiabatic equilibrium (*hp* constant) are initially placed on $x \le 0$ and $x \ge 0$, respectively. The unburned gas temperature is 300 K, and two pressure conditions of 1 and 10 atm are used. The initial profile is generated using an error function. The reaction mechanism of CH_4 is generated by GRI-Mech 3.0 [19], which consists of 53 species and 325 reactions. In Eq. (22), $\delta_L = 0.044$ cm and $T_{\rm ad} = 2224$ K for 1 atm and $\delta_L = 0.010$ cm and $T_{\rm ad} = 2267$ K for 10 atm are used.

Figure 1 shows the flame propagating speeds under 10 atm in terms of C_χ, where three LTF results having different grid sizes (320, 160, and 80 μm) and a DNS solution having the grid size of 5 μm are also plotted. The three LTF results demonstrate that a grid-independent solution is successfully achieved by using $C_\chi \gtrsim 50$, and are properly converged to the DNS solution even with coarser grid resolutions. Fig. 2 shows the number of grid points in a flame region that is defined by

$$N = \frac{(T_2 - T_1)/|\frac{{\rm d}T}{{\rm d}x}|_{\max}}{\Delta s_F}, \tag{23}$$

where T_1 is the temperature of unburned gas, and T_2 is the adiabatic flame temperature. The result indicates that, as analytically designed, the number of grid points in a flame region is almost identical for any grid size. Thus, it is demonstrated the LTF using Eq. (22) owns a grid-independent property of C_χ, which is preferable since the constant C_χ does not need to be adjusted depending on the employed grid size. The values of $C_\chi = 50 - 150$ are recommended. Almost identical results are also obtained for the pressure condition of 1 atm and a premixed H_2/air mixture. For reference, the results in the case of $n = 0$ in Eq. (17) are presented in the supplementary material. It is found that the solution significantly depends on employed grid sizes with $n = 0$.

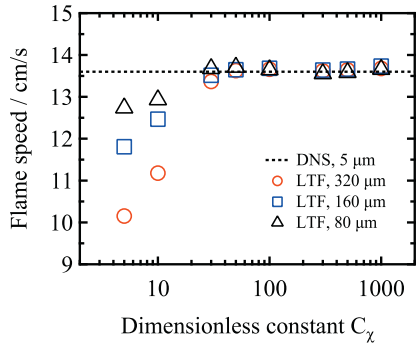

Fig. 1. Flame propagation speed under 10 atm in terms of the dimensionless constant, C_χ, for three different grid sizes.

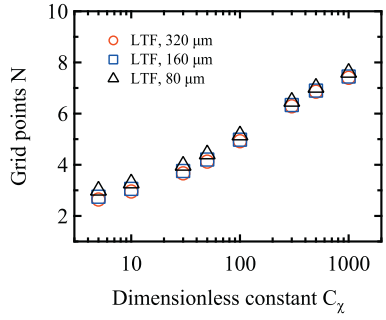

Fig. 2. Number of grid points in a flame region in terms of the dimensionless constant C_χ (for 10 atm).

3.2. Autoignition behavior in an open space

An advantage of the LTF, compared with the original TF model, may lie in the prediction capability of autoignition timing, because the LTF owns the automatic localization property through the use of the high-order derivative. Here, a simulation for the flame propagation induced by autoignition is carried out. The computational domain and boundary conditions are the same as those used in Section 3.1. The domain is filled with an unburned CH_4/air premixed mixture of 300 K under 1 atm. A high-temperature gas of 1500 K is inserted in

Please cite this article as: H. Terashima, Y. Hanada and S. Kawai, A localized thickened flame model for simulations of flame propagation and autoignition under elevated pressure conditions, Proceedings of the Combustion Institute, https://doi.org/10.1016/j.proci.2020.06.063

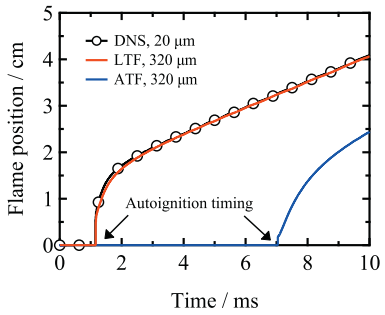

Fig. 3. Comparisons of flame propagation behaviors caused by autoignition. The original TF model is denoted as ATF.

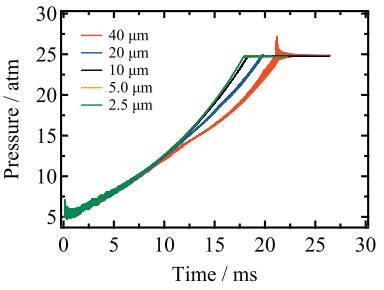

Fig. 4. Comparisons of time histories of pressure at the wall with no model at 600 K.

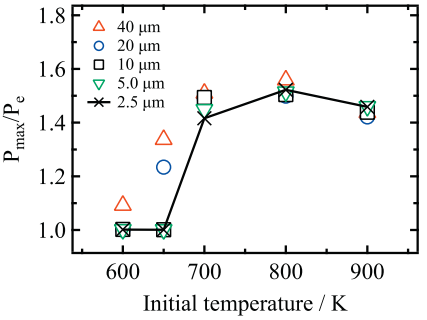

Fig. 5. Comparisons of knocking intensity with no model.

the region of $|x| \leq 1.0$ cm with an error function for autoignition. The dimensionless user-specified constant is $C_\chi = 100$, based on the results in Fig. 1.

Figure 3 shows the time history of the flame position in $x \geq 0$ region, in which the results obtained by a DNS having the grid size of 20 μm, the original TF model having a thickening factor of $(1 + \chi) = 5$ and the grid size of 320 μm, and the LTF having the grid size of 320 μm are compared. The result of the LTF agrees well with that of the DNS in terms of the autoignition timing occurring at $t = 1.1$ ms and the subsequent flame propagation. In contrast, the result of the original TF model shows a delay of autoignition timing because of the modification of the production rate by the thickening factor.

3.3. Flame propagation and end-gas autoignition in a confined space

A process relevant to knocking combustion is modeled by using a 1-D constant-volume reactor [14]. A symmetric condition is imposed on the left boundary, whereas the right boundary is adiabatic wall. A high-temperature kernel is initially introduced at the left boundary to induce a flame propagation. The initial pressure is 5 atm and the initial temperature changes from 600 K to 900 K. The reactor is initially filled with a stoichiometric n–C_4H_{10}/air premixed mixture. For the LTF in Eq. (22), $\delta_L = 0.0189$ cm and $T_{ad} = 2455$ K are used for all the conditions, which are estimated using a laminar flame under 5 atm and 600 K. The dimensionless user-specified constant is set to $C_\chi = 100$. The grid size is uniformly distributed. The detailed reaction mechanism is generated by KUCRS [20], where n–C_4H_{10} comprises 113 species and 426 reactions. More detailed information about this problem can be found in [14,18].

3.3.1. Results with no model

First, the result with no LTF is discussed. Fig. 4 shows the time histories of pressure at the wall, obtained using five grid sizes at 600 K. The pressure gradually increases according to the flame propagation in the confined space. Although no differences are observed during the initial stage, the difference caused by grid size becomes apparent from $t \approx 10$ ms. In the case of the maximum grid size of 40 μm, the increase of pressure becomes relatively slow, and a small pressure peak is eventually observed at approximately $t = 21$ ms. This indicates that the end-gas autoignition takes place because of the decrease of flame propagation speed. On the other hand, the pressure variation becomes steeper with smaller grid sizes, and no pressure peaks are observed. The pressure history is fully converged with the grid size of 5 μm. The results demonstrate that larger grid sizes are insufficient to properly resolve the thinning flame caused by the pressure increase in the reactor.

Figures 5 and 6 show the knocking intensity and timing obtained by changing the grid size. The knocking intensity is the ratio of the first peak pressure to the equilibrium pressure obtained from the time history of the maximum pressure in the reactor [14]. The disagreement of knocking intensity caused by the grid size appears at lower temperature conditions (e.g., 600 K and 650 K). The results of knocking timing also show that there are differences at lower temperature conditions. The slower flame propagation caused by the large grid size leads to the spurious occurrences of end-gas

Please cite this article as: H. Terashima, Y. Hanada and S. Kawai, A localized thickened flame model for simulations of flame propagation and autoignition under elevated pressure conditions, Proceedings of the Combustion Institute, https://doi.org/10.1016/j.proci.2020.06.063

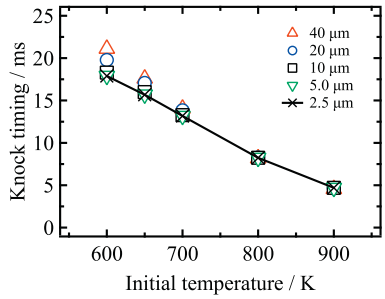

Fig. 6. Comparisons of knocking timing with no model.

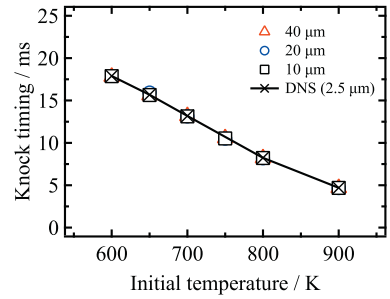

Fig. 9. Comparisons of knocking timing using LTF.

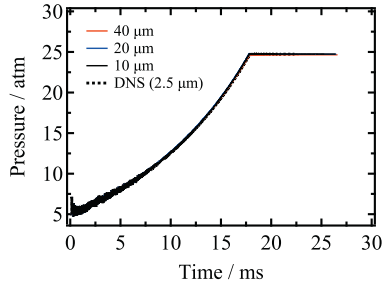

Fig. 7. Time histories of pressure at the wall by LTF in the case of 600 K.

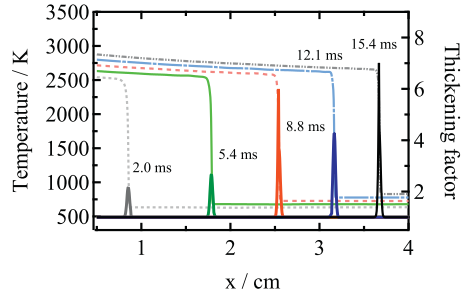

Fig. 10. Time histories of temperature (dashed lines) and thickening factor (solid lines) distributions using the grid size of 40 μm at 600 K.

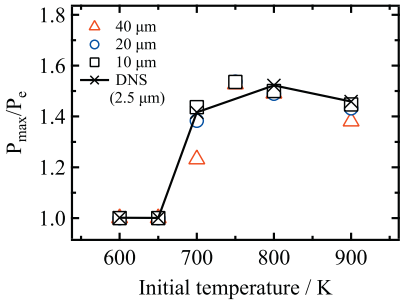

Fig. 8. Comparisons of knocking intensity using LTF.

autoignition. Below, the result having the minimum grid size of 2.5 μm is used as a reference solution.

3.3.2. *Results with LTF*

Figure 7 shows the pressure history at the wall obtained using the LTF, in which the results with three different grid sizes and the reference solution are plotted. In contrast to the result with no LTF, the LTF results with three grid sizes are almost identical and agree well with the reference solution.

The knocking intensity and timing obtained by using the LTF are shown in Figs. 8 and 9. The knocking occurrence is accurately predicted by using the LTF even on the larger grid sizes of 40 μm and 20 μm. At 700 K, the knocking intensity with the largest grid size of 40 μm is a bit smaller than the other knocking intensities. This is because the end-gas region at 700 K becomes very narrow. Therefore, the flame thickening affects the end-gas region and thus the autoignition timing through the modification of the production rate, which may be prevented by increasing the grid resolution near the end wall. The results demonstrate that the LTF provides the accurate prediction of flame propagation speed and end-gas autoignition timing under elevated pressure conditions, even on the coarse grid solutions.

Figure 10 presents a temporal sequence of the thickening factor, $(1 + \chi)$, and temperature profiles using the grid size of 40 μm at 600 K. It is found that the thickening factor is locally distributed in the flame region, and overall the peak becomes larger with the flame propagation. Fig. 11 shows the time histories of the maximum value of the thickening factor obtained using three grid sizes. All the results show that the maximum values automatically increase according to the thinning flame due to the elevated pressures. The automatic increase of the thickening factor demonstrates that the high-order derivative in the LTF model dynamically de-

Please cite this article as: H. Terashima, Y. Hanada and S. Kawai, A localized thickened flame model for simulations of flame propagation and autoignition under elevated pressure conditions, Proceedings of the Combustion Institute, https://doi.org/10.1016/j.proci.2020.06.063

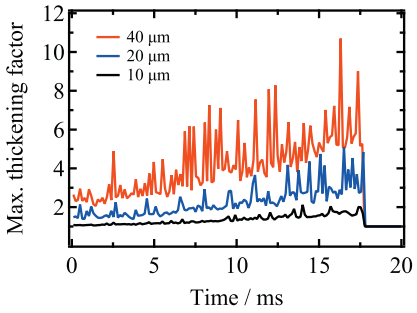

Fig. 11. Time histories of the maximum value of the thickening factor at 600 K with the effects of grid sizes.

tects the unresolved flames on the employed grids. Thus, the flame is dynamically thickened depending on the grid size to properly resolve the flame region. These results demonstrate the localization and dynamic operation properties of the LTF for capturing flame propagation and autoignition behaviors under elevated pressure conditions.

4. Conclusions

A localized thickened flame (LTF) model was proposed for the accurate prediction of flame propagation and autoignition using detailed chemical kinetics. The unresolved-scale components in the governing equations were consistently constructed, such that laminar flame speed is maintained on arbitrary grid sizes, while the flame is thickened. The model introduced the high-order derivative of temperature to localize the effect of the LTF in a flame region. The model parameter was determined by using grid size and laminar flame thickness to attain a grid-independent property. The 1-D laminar flame propagation problem in an open space determined an appropriate value of the user-specified constant in the model parameter and validated the performance of the LTF. The result using the 1-D constant-volume reactor demonstrated that the LTF successfully captures the flame propagation and end-gas autoignition behaviors under elevated pressure conditions, even on coarse grid resolutions. The thickening factor is locally distributed in the flame region, and the value automatically and dynamically is adjusted according to the change of flame thickness.

Declaration of Competing Interest

None.

Acknowledgments

This research was partially supported by JSPS KAKENHI grant nos. JP17K06939 and JP19K21927. We appreciate a contribution from a former graduate student, Yuya Takahashi (Tohoku Univ.), to the development of the LTF model.

Supplementary material

Supplementary material associated with this article can be found, in the online version, at doi:10.1016/j.proci.2020.06.063

References

[1] F. Perini, E. Galligani, R.D. Reitz, *Combust. Flame* 161 (2014) 1180–1195.
[2] Y. Morii, H. Terashima, M. Koshi, T. Shimizu, E. Shima, *J. Comput. Phys.* 322 (2016) 547–558.
[3] J.-H. Wang, S. Pan, X.Y. Hu, N.A. Adams, *Combust. Flame* 204 (2019) 397–413.
[4] S.B. Pope, *Prog. Energy Combust. Sci.* 11 (1985) 119–192.
[5] B. Thornber, R. Bilger, A. Masri, E. Hawkes, *J. Comput. Phys.* 230 (2011) 7687–7705.
[6] S. Menon, W.H. Calhoon, Jr, in: Symp. (Int.) Combust., volume 26, Elsevier, pp. 59–66.
[7] T. Butler, P. O'rourke, in: Symp. (Int.) Combust., volume 16, Elsevier, pp. 1503–1515.
[8] O. Colin, F. Ducros, D. Veynante, T. Poinsot, *Phys. Fluids* 12 (2000) 1843–1863.
[9] J.-P. Legier, T. Poinsot, D. Veynante, in: Proceedings of the summer program, volume 12, Center for Turbulence Research Stanford, CA,
[10] S. Yu, S. Navarro-Martinez, *Proc. Combust. Inst.* 35 (2015) 1955–1961.
[11] F. Proch, A. Kempf, *Proc. Combust. Inst.* 35 (2015) 3337–3345.
[12] O. Schulz, T. Jaravel, T. Poinsot, B. Cuenot, N. Noiray, *Proc. Combust. Inst.* 36 (2017) 1637–1644.
[13] T.B. Gatski, J.P. Bonnet, *Compressibility, Turbulence and High Speed Flow*, Academic Press, 2013.
[14] H. Terashima, M. Koshi, *Combust. Flame* 162 (2015) 1944–1956.
[15] F.A. Williams, *Combustion Theory*, CRC Press, 2018.
[16] A.W. Cook, W.H. Cabot, *J. Comput. Phys.* 195 (2004) 594–601.
[17] S. Kawai, S.K. Lele, *J. Comput. Phys.* 227 (2008) 9498–9526.
[18] H. Terashima, A. Matsugi, M. Koshi, *Combust. Flame* 184 (2017) 324–334.
[19] G. Smith, D. Golden, M. Frenklach, N. Moriarty, B. Eiteneer, M. Goldenberg, C. Bowman, R. Hanson, S. Song, W. Gardiner Jr, V. Lissianski, Z. Qin, GRI-Mech 3.0, http://combustion.berkeley.edu/gri-mech/version30/text30.html, (2000).
[20] A. Miyoshi, KUCRS software library. see the web: http://akrmys.com/KUCRS/ for update information, 2011.

Please cite this article as: H. Terashima, Y. Hanada and S. Kawai, A localized thickened flame model for simulations of flame propagation and autoignition under elevated pressure conditions, Proceedings of the Combustion Institute, https://doi.org/10.1016/j.proci.2020.06.063